Remote Sensing of Environment 113 (2009) 2424–2430

Contents lists available at ScienceDirect

Remote Sensing of Environment

journal homepage: www.elsevier.com/locate/rse

A class-based approach to characterizing and mapping the uncertainty of the MODIS ocean chlorophyll product

Timothy S. Moore [a,*], Janet W. Campbell [a], Mark D. Dowell [b]

[a] Ocean Process Analysis Laboratory, University of New Hampshire Durham, NH 03824, USA
[b] European Commission, Joint Research Centre, Institute for Environment and Sustainability TP 272, via E. Fermi 2749, I-21027, Ispra (VA), Italy

ARTICLE INFO

Article history:
Received 9 April 2009
Received in revised form 9 July 2009
Accepted 10 July 2009

Keywords:
Chlorophyll *a*
Ocean color
Algorithms
Bio-optics
Uncertainty

ABSTRACT

Global chlorophyll products derived from NASA's ocean color satellite programs have a nominal uncertainty of ±35%. This metric has been hard to assess, in part because the data sets for evaluating performance do not reflect the true distribution of chlorophyll in the global ocean. A new technique is introduced that characterizes the chlorophyll uncertainty associated with distinct optical water types, and shows that for much of the open ocean the relative error is under 35%. This technique is based on a fuzzy classification of remote sensing reflectance into eight optical water types for which error statistics have been calculated. The error statistics are based on a data set of coincident MODIS Aqua satellite radiances and *in situ* chlorophyll measurements. The chlorophyll uncertainty is then mapped dynamically based on fuzzy memberships to the optical water types. The uncertainty maps are thus a separate, companion product to the standard MODIS chlorophyll product.

1. Introduction

Since the era of the Coastal Zone Color Scanner 30 years ago, empirical algorithms — currently represented by OC4v4 for SeaWiFS and OC3M for MODIS (O'Reilly et al., 2000) — have served as the basis for the standard chlorophyll *a* (*Chl*) products derived from NASA's ocean color satellite sensors. These algorithms are based on statistically-derived relationships between *Chl* and the ratio of water-leaving radiance in two or more spectral bands. Such algorithms, parameterized from *in situ* data, are currently used operationally to produce global maps of *Chl*. Characterizing the uncertainty of global *Chl* products has important consequences for the uncertainty budgets of higher order algorithms that use *Chl* as an input product (e.g., primary production algorithms), and in assessing trends from long-term data records across satellite and mission platforms.

The desired level of accuracy for satellite-derived *Chl* is ±35% relative to the value measured in the field (McClain et al., 2006; Bailey & Werdell, 2006; Hooker et al., 1992). Currently, the average relative error of the global chlorophyll product, defined as the mean of the absolute difference between measured *Chl* and the derived *Chl*, exceeds 35%. [Although we use the term 'error', in the context of product performance we are actually evaluating 'uncertainty', since error assumes that truth is known. In practice, measured chlorophyll has its own error or uncertainty. Thus, we are more correctly speaking of uncertainty, but the term 'error' is used herein when speaking of the derived absolute difference.] Algorithm errors have been assessed using the NOMAD data set (Werdell & Bailey, 2005) in which *in situ* radiometric measurements are made coincident with chlorophyll. Like most *in situ* data sets, NOMAD has a disproportionate amount of high chlorophyll data relative to the global distribution, because there are more data collected in coastal regions than in the open ocean. The large errors associated with high chlorophyll data (*Chl*>1 mg m^{-3}) inflate the overall error calculated from the NOMAD data (Fig. 1). After weighting the errors shown in Fig. 1 by the global chlorophyll distribution from the SeaWiFS climatology (1997–2005), the average relative algorithm error is about 36%.

Ultimately, the uncertainty of the satellite chlorophyll products must also include the uncertainty associated with other sources. The NOMAD analysis only treats the algorithm accuracy relative to measurements made at the same station by standard oceanographic methods. Specifically, they do not account for errors associated with the atmospheric correction or mismatches in spatial scale (the pixel area versus a single point). We have estimated errors using a smaller data set, the Aqua validation data set (Werdell & Bailey, 2005), consisting of 541 satellite radiances matched with *in situ* chlorophyll measurements. The average absolute error based on this data set is 73%. However, focusing on just one number for the uncertainty of the global chlorophyll product does not provide any information on its geographic distribution.

An alternative to representing the error characteristic with a single, bulk statistic is to represent the error for different trophic states as determined by the chlorophyll level.

The disadvantage of this approach is that chlorophyll is not the only water constituent affecting the radiometric signal, and thus the relationship of that signal to the chlorophyll concentration. Other optically active

* Corresponding author.
E-mail address: timothy.moore@unh.edu (T.S. Moore).

0034-4257/$ – see front matter © 2009 Elsevier Inc. All rights reserved.
doi:10.1016/j.rse.2009.07.016

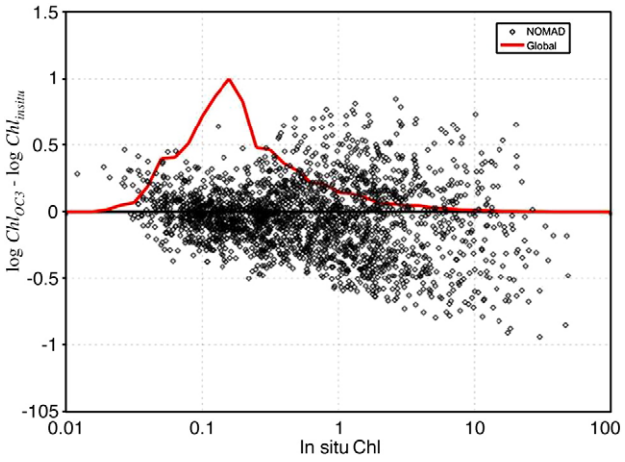

Fig. 1. OC3M log errors plotted against *in situ* chlorophyll from the NOMAD data set (Werdell & Bailey, 2005). The red curve is the frequency distribution of *Chl* from the SeaWiFS climatology for 1997–2005. This reveals that the smallest errors occur in the vicinity of the mode of the climatological distribution.

constituents affecting the algorithm uncertainty would not be accounted for in a scheme involving trophic states based strictly on the chlorophyll level.

Historically, ocean color remote sensing techniques have been based on two optical water types, known as "Case 1" and "Case 2" (Morel & Prieur, 1977). Here we present an approach whereby errors are characterized for eight distinct water types defined by their optical properties. This approach has the advantage that it operates directly on the radiance measurements, and provides a mechanism to map the optical water types from ocean color satellite data at any resolution. Thus, any chlorophyll product operationally produced would have a companion chlorophyll uncertainty map at the same spatial and temporal resolution. The approach can be extended to other derived products and algorithms, such as the family of semi-analytic algorithms.

Our motivation is to characterize the uncertainty distribution in the MODIS chlorophyll product and to map it dynamically at the global scale. This analysis uses the Aqua validation data set to characterize the uncertainty, and the radiance data from MODIS Aqua to map the uncertainty. It will be demonstrated using Aqua data from 2005.

2. Methods

The overall approach required three steps — 1) identifying the optical water types, 2) characterizing uncertainty for each water type, and 3) mapping the water types and associated uncertainties from satellite ocean color data. To perform step 1, an *in situ* data set of remote sensing reflectance was used in conjunction with a clustering algorithm to identify the optical water types. The optical water types are thus defined by the statistical properties of their associated remote sensing reflectance spectra, which serve as the basis for classifying other measurements of remote sensing reflectance. These could be other *in situ* measurements or satellite ocean color data. The characterization of the uncertainty of *Chl* for each water type is performed in step 2, where a second, independent data set is classified into the optical water types using the statistics from step 1. For each optical water type, *Chl* uncertainty statistics were derived based on the *Chl* data within each water type subset. For step 3, optical water types were identified from satellite data using the same classification technique as step 2. In this step, however, the classification is based on fuzzy memberships, which serve as weighting factors to the water type-specific uncertainty values which ultimately are mapped at the satellite input scale. Step one occurs once and forms a standardized baseline to which any satellite or *in situ* data set can be compared (in steps 2 and 3). The characterization of *Chl* uncertainty ideally is platform- and algorithm-specific, and should be performed independently for each sensor/algorithm. Step 3 is specific to each sensor and is the operational aspect of the method, and can be applied to any ocean color sensor at any level of resolution.

2.1. Data sets

The NOMAD version 2 data set (adapted from Werdell & Bailey, 2005) was used as the primary source of data for the identification of the optical water types based on remote sensing reflectance (step 1). This is a global *in situ* data set archived by NASA and assembled from data sets contributed by dozens of investigators. The global data set includes the upper-layer chlorophyll *a* concentration measured fluorometrically, together with coincident measurements of water-leaving radiance and downwelling surface irradiance in 20 visible-range spectral bands. The remote sensing reflectance was calculated as the ratio of the upwelling radiance to the downwelling irradiance for all bands. The data set was reduced from 4459 to 2372 points after quality control.

The Aqua validation data set (Bailey & Werdell, 2006) was used to characterize the OC3M *Chl* uncertainty statistics. This data set consists of Aqua MODIS satellite radiances averaged over 5×5 pixel boxes and *in situ* chlorophyll measurements made within 3 h of the satellite overpass. The radiance data provided for this analysis were atmospherically corrected and normalized for input to the OC3M algorithm (Bailey, pers. comm.). The number of points in this data set was 541. These data were classified into the water types identified from the much larger NOMAD data set. Station locations for both data sets are shown in Fig. 2. The same water types were identified in a SeaWiFS validation data set which contained considerably more data points ($N = 1576$). Although the uncertainty in the SeaWiFS *Chl* product is not the subject of this paper, a comparison was made with the MODIS *Chl* uncertainties associated with the same water types.

For step 3, a global time series of monthly composites of MODIS Aqua satellite data from 2005 at 4-km resolution were obtained from the NASA Ocean Color data archive (oceancolor.gsfc.nasa.gov). The products required for this analysis were the normalized radiance fields at 412, 443, 489, and 551nm. When the method is used operationally, it can be applied at the level-2 processing stage to derive the uncertainty associated with each chlorophyll retrieval. The uncertainty statistics can then be composited along with the chlorophyll to derive level-3 uncertainty maps.

2.2. Optical classification and error analysis

Optical water types representative of the global ocean were determined from the NOMAD V2 data set using the fuzzy *c*-means clustering (FCM) algorithm. This methodological approach is identical to that of Moore et al. (2001), although using a global data set versus a regional data set. The reason for using the FCM algorithm instead of other clustering algorithms is the availability of *validity functions* (Bezdek et al. 1997, Wu & Yang, 2005) to assess the optimal number of clusters (c). Like many data sets, the number of clusters in the NOMAD remote sensing reflectance data set is unknown. Clustering algorithms usually require this parameter to be set prior to clustering. Validity functions are a family of mathematical functions that measure performance aspects of a clustering result, such as the distance between clusters (separation) and the distribution of points around a cluster (compactness). The strategy typically used is to cluster the data over a range of c values and evaluate each clustering result with the validity functions. Since no single validity function is perfect for all data sets, it is common to use multiple validity functions and poll them for the optimal value of c. This optimal value is then chosen based on the highest number of 'votes' from the validity functions. In this analysis, 12 different validity functions were used and all selected eight clusters

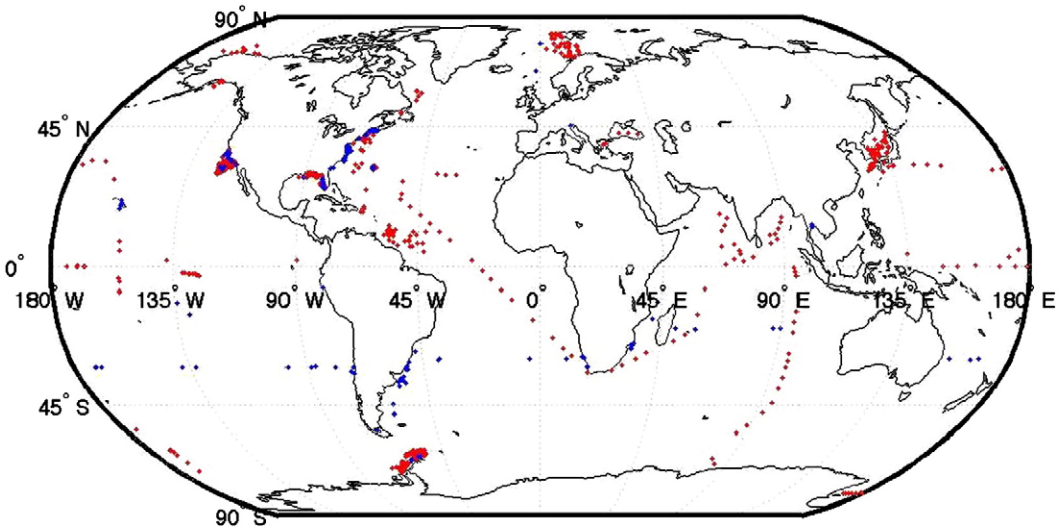

Fig. 2. Geographic distribution of the NOMAD V2 data set (red) and the Aqua validation data set (blue) used in this analysis.

(i.e., *optical water types*) as being optimal. These eight water types were identified (Fig. 3), and sequentially numbered along the general trend of increasing chlorophyll and optical complexity. They range from low-chlorophyll, blue-waters (types 1 and 2) to turbid, sediment-dominated waters (types 6–8).

The spectral radiances within each water type were statistically characterized (i.e., means and covariances derived), and these statistics were used to define the fuzzy membership function for each water type. The fuzzy membership function is: $1 - F(Z^2)$, where Z^2 is a squared Mahalanobis distance and F is a cumulative chi-square distribution. The Mahalanobis distance is the multivariate equivalent of the standardized random variable $Z = (X - M)/S$, which is the distance of the univariate random variable X from its mean M normalized by the standard deviation S. In other words, the Mahalanobis distance is a weighted form of the Euclidean, and is preferable because it incorporates the shape of the distribution of points around the cluster center (i.e., the geometric shape of the point cloud expressed in terms of variance). The fuzzy membership ranges from 0 to 1 and depicts the degree to which a measured radiance vector belongs to a given optical water type. It has the value 1 if the measured radiance vector is identical to the mean radiance of that water type, and its value diminishes to zero as the Mahalanobis distance increases.

Fuzzy memberships to the eight water types were calculated for each of the radiance vectors in the Aqua validation data set, and then the data were assigned to the water type having the maximum fuzzy membership (i.e., each point was assigned to only one water type). For each subset representing an optical water type, error statistics were calculated for the relative absolute error and the log error of the chlorophyll retrieval. These statistics represent the MODIS chlorophyll uncertainty in different ways. The log error was the metric minimized when the OC3M algorithm was parameterized as a fourth-order polynomial, and it is the error seen as the scatter in Fig. 3. It retains the sign of the error, but its units are decades of log. The relative absolute error, expressed as a percentage of the measured chlorophyll, is easier to interpret but does not retain the sign.

To arrive at global maps of the uncertainty, fuzzy memberships to the optical water types were calculated using Aqua MODIS ocean color radiance data. In this case, the same membership function was used as for the Aqua validation set, but the fuzzy memberships were not hardened. The fuzzy memberships for each pixel normalized by their sum then served as weighting factors for the error characteristics from each water type. Thus, the radiance classes and the fuzzy membership function provide a mechanism for mapping uncertainties at the same scale as the ocean color imagery.

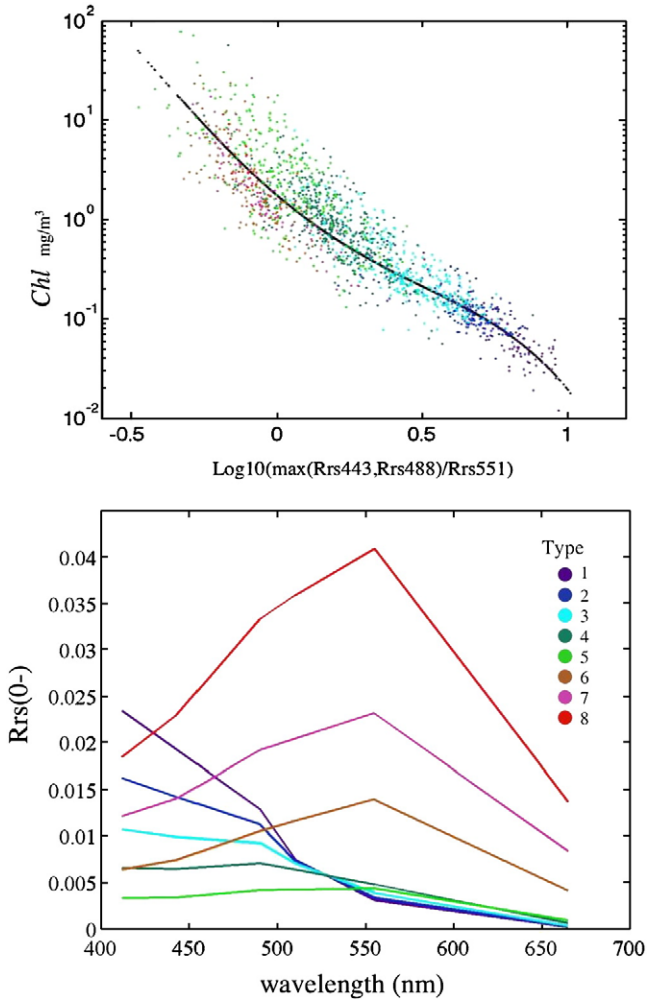

Fig. 3. Top: The statistical relationship between *Chl* and the reflectance ratio used to define the OC3M algorithm. The point data are from the NOMAD V2 data set, and the line is the OC3M algorithm. Points are color-coded according to the optical water type having the highest membership (see text). Bottom: the mean reflectance spectra for the eight optical water types.

3. Results

The distributions of the eight optical water types are indicated by the colors in the statistical relationship defining the OC3M algorithm shown in Fig. 3 (top). Although there is the general pattern of increasing *Chl* from type 1 to type 8, the chlorophyll ranges overlap between water types. These optical water types differ significantly in their spectral reflectance shapes and magnitudes (Fig. 3 (bottom)). It is clear that they represent very different optical environments despite a similar range of chlorophyll levels, which is most evident in water types 4–8. The fundamental advantage of this approach is that the optical water types, distinguished by their spectral properties, can have similar or overlapping chlorophyll ranges. This recognizes waters of differing composition that have the same chlorophyll concentration but distinct optical properties.

The scatter of points about the OC3M curve in Fig. 3 (top) represents only the algorithm uncertainty. This includes uncertainties associated with the measurements and the algorithm itself. It is based solely on *in situ* radiometric and chlorophyll measurements, and therefore does not include any uncertainty attributed to atmospheric correction or satellite radiance accuracy. These additional uncertainties are included when basing error statistics on the validation data sets. A comprehensive error analysis was made using the Aqua validation data set (Table 1). The average relative error of the eight optical water types ranged from 16% to 123%. Only type 1 meets the NASA criterion for 35% relative accuracy. The uncertainty statistics for the same water types using the SeaWiFS validation data set are shown in Table 2 for comparison purposes. The same general trends are exhibited across the water types as for the Aqua data set.

As expected, there is an overall trend of lower errors associated with the 'blue-water' types (1–3) compared to the more optically complex waters (4–8). This was predictable, as the optical properties of types 4–8 become increasingly influenced by suspended sediments and organic matter. There is an over-representation of data points from water types 4–8 in this data set (as in NOMAD), and consequently the overall mean relative error — 73% — overestimates error in the blue-water types. Thus, the bulk error statistic is not representative of the global ocean, and gives a misleading and pessimistic view of the uncertainty associated with the Aqua MODIS chlorophyll product.

Distinction among the optical water types is evident when their spatial distributions are taken into account. Their geographic distribution in May 2005, as shown by their fuzzy memberships in Fig. 4, is typical. Types 1–3 occupied more than 84% of the surface area of the oceans in this month. These blue-water types are found in the open ocean basins, while types 5–8 are constrained to near-shore, coastal environments with a much smaller geographic footprint. Water type 1 is found in the central gyres. It is surrounded by type 2 and then type 3. Water type 4 is found in various high *Chl* regions, including the North Atlantic (spring bloom) and near upwelling regions (e.g., Benguela, Peru).

The global distribution of the chlorophyll uncertainty is shown in Fig. 5 for four months in 2005. Water type 1 represents more than 30% of the ocean in these months, and it has a relative *Chl* error well under 35%. The fuzzy membership functions are able to capture the dynamic behavior of the ocean by assigning a given pixel to one or more of the optical water types based solely on the pixel's reflectance spectrum. Since a pixel's reflectance spectrum varies over time (i.e., from one sequential image to another), its membership to the optical water types will vary. In this approach, the membership functions capture the dynamic behavior of the ocean through its optical properties and thus allow a dynamic characterization of the chlorophyll uncertainty. The end result is a new product that can be operationally produced at any level (i.e., time and spatial scale) of satellite imagery, and is to be delivered in conjunction with the MODIS chlorophyll product. This technique is equally applicable to high resolution (1 km), single pass images as to global composites at 8-day or monthly time scales. To apply the method proposed here to any ocean color satellite product, one must know the mean and covariance properties of reflectance for each of the eight water types. These statistics were derived in Step 1 of the method, and are presented in the Appendix. They can be used to compute the memberships of any reflectance data set to the eight optical water types.

Table 1
Uncertainty statistics of the eight optical water types for the MODIS *Chl* product as characterized using the Aqua validation data set.

Optical water type	Average relative error (%)	RMS log error	Bias log error	# points	Average Chl	Min Chl	Max Chl
1	16	0.090	−0.002	37	0.075	0.033	0.147
2	48	0.252	−0.125	33	0.257	0.077	0.703
3	51	0.265	−0.033	23	0.361	0.090	0.748
4	68	0.280	0.066	132	2.45	0.05	29.00
5	60	0.259	0.041	105	2.27	0.25	19.93
6	123	0.366	0.216	104	7.05	0.46	29.05
7	52	0.297	0.046	14	1.05	0.29	6.12
8	81	0.307	0.116	93	9.97	0.96	50.84
All	73	0.289	0.078	541	4.17	0.033	50.84

Table 2
Uncertainty statistics of the eight optical water types for the SeaWiFS *Chl* product as characterized using the SeaWiFS validation data set.

Optical water type	Average relative error (%)	RMS log error	Bias log error	# points	Average Chl	Min Chl	Max Chl
1	35	0.302	0.087	35	0.075	0.030	0.89
2	53	0.260	−0.059	173	0.257	0.024	0.77
3	35	0.216	0.029	103	0.361	0.078	2.60
4	73	0.283	−0.083	235	2.45	0.05	8.38
5	77	0.273	−0.063	371	2.27	0.147	19.85
6	93	0.319	−0.152	540	7.05	0.14	129.3
7	95	0.314	−0.174	114	1.05	0.056	22.70
8	110	0.589	0.138	5	9.97	0.65	3.40
All	77	0.292	−0.094	1576	3.52	0.147	23.48

4. Discussion

Classes based on spectral radiance have been used in land cover remote sensing (Wang, 1990) and remote mineral spectroscopy (Mustard & Pieters, 1989). In these applications, observed radiance spectra are considered to be a combination of end-member spectra that are obtained from homogenous samples of various substrates (e.g., forest, desert, olivine, magnetite). Sample observations or image pixels have been assigned partial membership to the end members using mixture models (Mustard & Pieters, 1989) and fuzzy classification schemes (Wang, 1990) where the fuzzy memberships can be viewed as the proportion of the end-member substrate present. In these two examples (land cover and mineral spectroscopy) the systematics of the spectral mixing is quite different. In the case of land cover, the combination of the end-member spectra is *macroscopic*, where individual components occur as discrete homogeneous patches within a pixel. Here, the overall pixel reflectance is a linear combination of the end members present within the pixel (Mustard & Pieters, 1989). In the case of mineral spectroscopy, the reflectance observations are from *microscopic* or *intimate* mixtures, where the minerals are randomly distributed and there is multiple light scattering among the minerals present. The observed reflectance is a non-linear combination of end members in this case (Johnson et al., 1983; Hapke, 1981).

Neither of these views is appropriate for the optical water type classes we have described in this paper. An ocean reflectance spectrum is the result of a microscopic mixture of constituents, and like the case of mineral spectroscopy, the spectrum can be modeled as a non-linear function of the constituent concentrations. However, the reflectance classes described here do not represent pure end members, but are the result of a clustering algorithm that found structure within a reflectance data set.

In some respects, it is tempting to view the fuzzy memberships in the macroscopic sense as representing the proportion of each class within the pixel, but this interpretation is not satisfactory either. It would imply that with finer spatial resolution, one could differentiate the end-member classes within the pixel. This is not the case in the

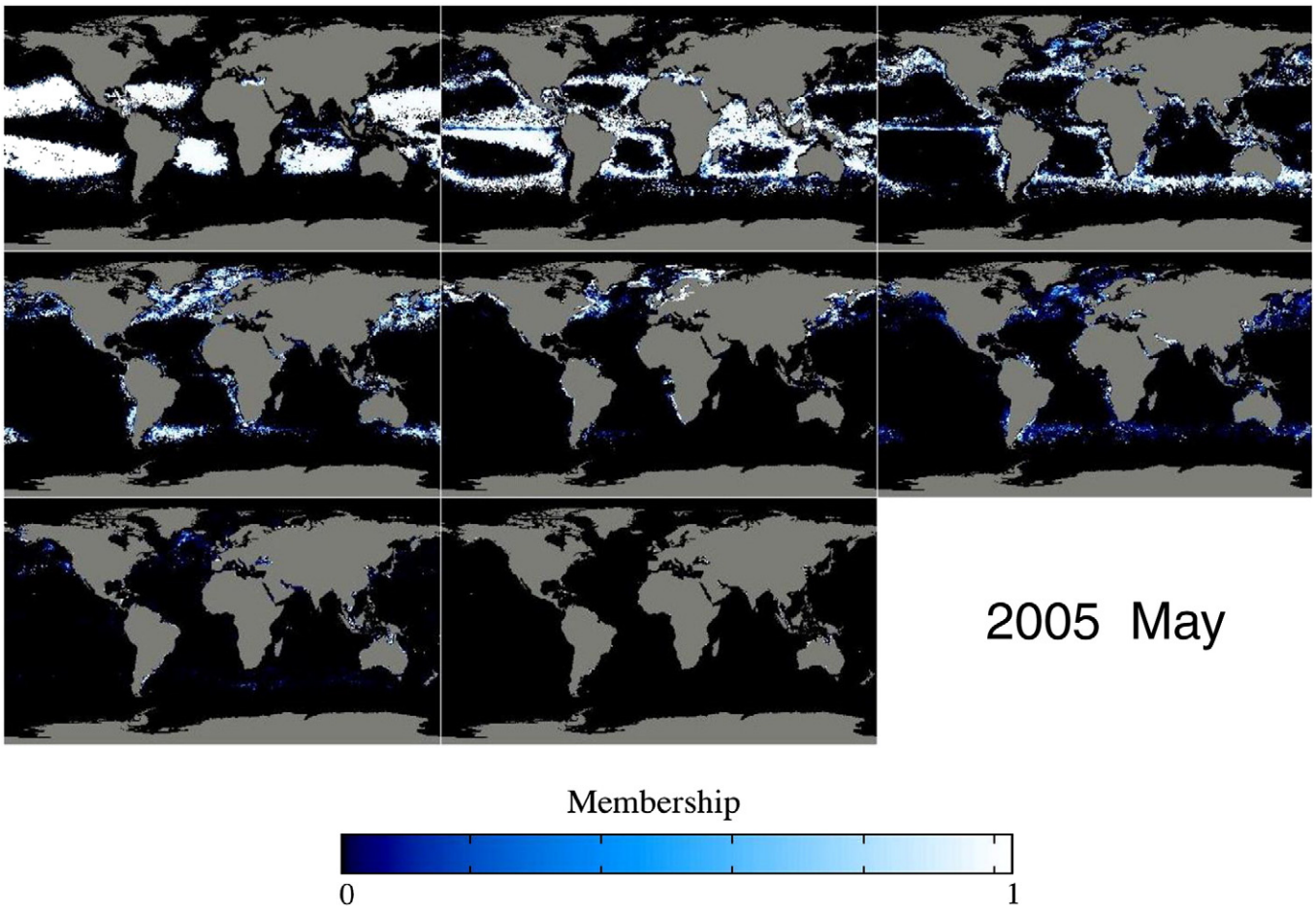

Fig. 4. The fuzzy membership maps of the eight optical water types for a monthly composite satellite image from MODIS Aqua for May 2005. From left to right, types 1–3 are top row; types 4–6 are middle row, and types 7–8 are bottom row. Memberships have been normalized by the sum.

ocean because of the intimate mixing of waters at the microscopic scale. In fact, we caution against the notion of end members in this context. However, the functional use of the water types is equivalent to an 'end member' as used in the membership function. Despite the fact that we have identified water types with clearly different reflectance and by default optical properties, we have refrained from

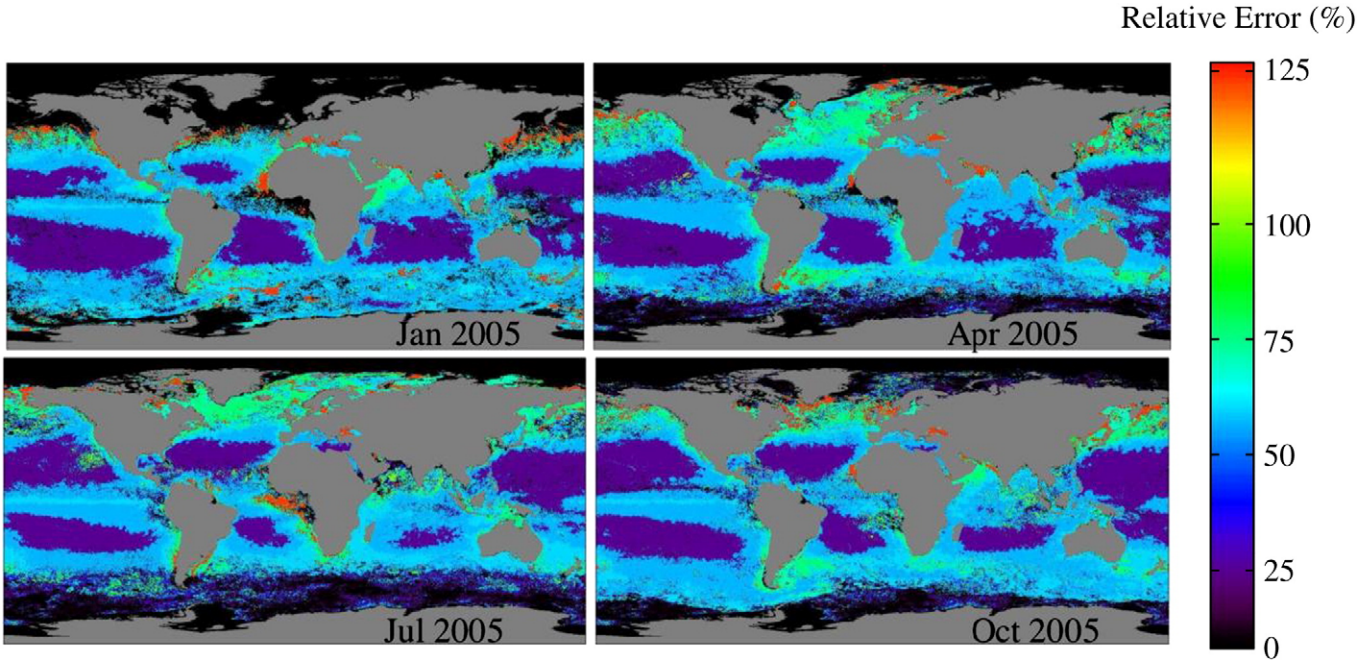

Fig. 5. Global maps of the MODIS Aqua chlorophyll uncertainty for January, April, July, and October 2005.

labeling the water types other than calling them water types 1 through 8. While descriptive labels are primarily a convenient way of identifying the classes, they have no real quantitative basis in the *in situ* data, given the limited information about phytoplankton community structure or other constituents.

This approach has several advantages compared to other methods, including methods based on the chlorophyll value itself. First, the optical water types are based on the fundamental measurement of the ocean color satellite — namely radiance rather than a derived product, such as chlorophyll. The optical water type method affords the ability to differentiate optical waters with overlapping chlorophyll ranges. The higher chlorophyll values can belong to one of several different optical water types (e.g., water types 4–6). These water types have points within the same chlorophyll range (Fig. 3 (top)) but differ with respect to other optically active constituents. However, uncertainty can differ by a factor of two for these water types (Table 1), ranging from 60% (type 5) to 123% (type 6). These two water types characterize very different water masses — type 5 being that of highly absorbing waters (either from phytoplankton or CDOM), and type 6 more typical of a high scattering type (either from sediments or other particles). The ability to differentiate these water types is particularly valuable in coastal regions where all these water types are found. Uncertainty based on chlorophyll would not have this capability.

The method demonstrated here utilized three data sets. A large *in situ* data set (NOMAD v2, $N=2372$) was used to identify and statistically characterize eight optical water types. Statistics of the water types' radiance spectra were the basis for defining fuzzy membership functions which were then applied to the satellite radiance measurements to determine membership to the eight optical water types. The Aqua validation data set ($N=541$) was used to characterize error statistics for each of the water types after sorting the data according to their maximum fuzzy membership. By using this data set to characterize errors, errors from all sources are included in the uncertainty. Finally, MODIS Aqua radiance data were used as input to the fuzzy membership functions to map the optical water types globally, and to estimate the uncertainty as a weighted average of memberships of the water types present at each pixel.

The optical water types were the result of an objective sub-setting process (i.e., clustering) of the NOMAD v2 data set. As more data are added to the NOMAD data set, characteristics of the optical water types will evolve and eventually converge to a stable set. In fact, an earlier set of water types identified from predecessor data sets to NOMAD V2 had slightly different mean reflectance spectra but the same number of types. Given the size of the NOMAD data set used in this analysis, we believe that the statistics defining the water types are reasonably stable already.

The Aqua validation data set, on the other hand, is now limited in size and more data are clearly needed. As data are added to the Aqua validation data set, the error characterization for the MODIS chlorophyll product will improve. The SeaWiFS validation data set is approximately three times larger than that of Aqua, reflecting the longer operation of the sensor. We predict that the error characterization for Aqua (Table 1) will eventually be similar to that of SeaWiFS (Table 2) as more Aqua data are added.

While statistical distributions for both the optical water types and their uncertainty characterization may not be final, the framework is there for future growth and also for applying the method to other ocean color algorithms and products. This provides a bridge to link the uncertainties between sensors that will be essential for developing long-term data records originating from different sensors and algorithms.

In this context, the eight optical water types serve as the common base. For application to other sensors or algorithms, it is recommended that product uncertainties be derived from matchup validation data sets as shown with the Aqua and SeaWiFS validation data sets, since they include all sources of uncertainties in the product (algorithm, atmospheric, and radiometric) as opposed to strictly using an *in situ* data set such as the NOMAD V2 data set which only yields algorithm uncertainty. Although we focused on the OC3M algorithm and the use of the Aqua validation data set, we also provided uncertainty values for the SeaWiFS OC4v4 algorithm using the SeaWiFS validation data. For the MERIS chlorophyll product, a separate validation data set would be required that contained *in situ* chlorophyll measurements and satellite-matched radiances. This approach is also applicable to semi-analytic algorithms and other ocean color products, such as the diffuse attenuation coefficient. In all cases, matchup data are required to produce the full product uncertainty.

5. Summary

A framework for characterizing the uncertainty of the products derived from ocean color satellite measurements is presented. This approach provides a mechanism for assessing uncertainty associated with distinct optical water types that have been identified in a global *in situ* optical data set. The optical water types can be mapped dynamically in satellite ocean color imagery, and the uncertainty of algorithm retrievals can be prescribed at the same spatial scale as the satellite image. Based on this analysis for MODIS Aqua, only *Chl* retrievals in the ocean gyres meet the 35% relative error criterion set by NASA. The same methodology could be applied to other satellite products, and thus provide a common basis for determining uncertainty. The method is particularly suited for the dynamic oceanic environment as it allows uncertainty maps to vary in time and space in concert with the satellite-derived chlorophyll distributions.

Acknowledgments

The authors would like to thank Sean Bailey and Jeremy Werdell for providing the satellite radiance mathcups for the SeaWiFS and Aqua validation data sets.

Appendix

Table A1
Subsurface remote sensing reflectance (Rrs(0-)) spectral means for the eight water types at the 6 SeaWiFS wavelengths.

Optical type	Rrs 410	Rrs 443	Rrs 490	Rrs 510	Rrs 555	Rrs 670
1	0.0234	0.0192	0.0129	0.0075	0.0031	0.0002
2	0.0162	0.0141	0.0112	0.0073	0.0034	0.0002
3	0.0107	0.0098	0.0092	0.0070	0.0039	0.0003
4	0.0065	0.0064	0.0070	0.0064	0.0048	0.0006
5	0.0033	0.0034	0.0042	0.0042	0.0043	0.0009
6	0.0064	0.0074	0.0105	0.0116	0.0140	0.0041
7	0.0121	0.0140	0.0192	0.0204	0.0231	0.0084
8	0.0184	0.0230	0.0333	0.0359	0.0409	0.0137

Table A2
Covariance matrices for optical water types.

Type 1					
0.00000959	0.00000556	0.00000138	−0.00000034	−0.00000024	−0.00000003
0.00000556	0.00000493	0.00000193	0.00000060	0.00000023	0.00000001
0.00000138	0.00000193	0.00000282	0.00000223	0.00000119	0.00000007
−0.00000034	0.00000060	0.00000223	0.00000232	0.00000119	0.00000007
−0.00000024	0.00000023	0.00000119	0.00000119	0.00000071	0.00000005
−0.00000003	0.00000001	0.00000007	0.00000007	0.00000005	0.00000001
Type 2					
0.00000346	0.00000186	−0.00000011	−0.00000060	−0.00000062	−0.00000005
0.00000186	0.00000228	0.00000086	0.00000033	−0.00000007	0.00000003
−0.00000011	0.00000086	0.00000231	0.00000221	0.00000145	0.00000023
−0.00000060	0.00000033	0.00000221	0.00000266	0.00000191	0.00000034
−0.00000062	−0.00000007	0.00000145	0.00000191	0.00000175	0.00000041
−0.00000005	0.00000003	0.00000023	0.00000034	0.00000041	0.00000021

(continued on next page)

Table A2 (*continued*)

Type 3					
0.00000241	0.00000144	0.00000035	−0.00000031	−0.00000063	−0.00000006
0.00000144	0.00000138	0.00000076	0.00000015	−0.00000021	−0.00000001
0.00000035	0.00000076	0.00000161	0.00000156	0.00000121	0.00000016
−0.00000031	0.00000015	0.00000156	0.00000227	0.00000209	0.00000031
−0.00000063	−0.00000021	0.00000121	0.00000209	0.00000225	0.00000037
−0.00000006	−0.00000001	0.00000016	0.00000031	0.00000037	0.00000013
Type 4					
0.00000166	0.00000091	0.00000034	−0.00000009	−0.00000080	−0.00000025
0.00000091	0.00000097	0.00000071	0.00000025	−0.00000041	−0.00000015
0.00000034	0.00000071	0.00000118	0.00000103	0.00000072	0.00000003
−0.00000009	0.00000025	0.00000103	0.00000137	0.00000162	0.00000025
−0.00000080	−0.00000041	0.00000072	0.00000162	0.00000290	0.00000065
−0.00000025	−0.00000015	0.00000003	0.00000025	0.00000065	0.00000050
Type 5					
0.00000178	0.00000132	0.00000104	0.00000081	0.00000018	−0.00000014
0.00000132	0.00000127	0.00000121	0.00000099	0.00000034	−0.00000010
0.00000104	0.00000121	0.00000150	0.00000142	0.00000110	0.00000013
0.00000081	0.00000099	0.00000142	0.00000158	0.00000177	0.00000042
0.00000018	0.00000034	0.00000110	0.00000177	0.00000351	0.00000131
−0.00000014	−0.00000010	0.00000013	0.00000042	0.00000131	0.00000081
Type 6					
0.00000715	0.00000586	0.00000409	0.00000292	0.00000005	−0.00000075
0.00000586	0.00000589	0.00000520	0.00000398	0.00000027	−0.00000114
0.00000409	0.00000520	0.00000634	0.00000541	0.00000188	−0.00000097
0.00000292	0.00000398	0.00000541	0.00000528	0.00000392	0.00000070
0.00000005	0.00000027	0.00000188	0.00000392	0.00000995	0.00000657
−0.00000075	−0.00000114	−0.00000097	0.00000070	0.00000657	0.00000819
Type 7					
0.00002625	0.00001981	0.00001058	0.00000544	−0.00000654	−0.00001122
0.00001981	0.00001745	0.00001314	0.00000822	−0.00000431	−0.00001228
0.00001058	0.00001314	0.00001629	0.00001226	0.00000035	−0.00001311
0.00000544	0.00000822	0.00001226	0.00001170	0.00000742	−0.00000500
−0.00000654	−0.00000431	0.00000035	0.00000742	0.00002241	0.00001782
−0.00001122	−0.00001228	−0.00001311	−0.00000500	0.00001782	0.00003987
Type 8					
0.00001186	0.00001134	0.00001139	0.00000919	0.00000395	−0.00000186
0.00001134	0.00001484	0.00002034	0.00001907	0.00001531	0.00000087
0.00001139	0.00002034	0.00003467	0.00003546	0.00003555	0.00000708
0.00000919	0.00001907	0.00003546	0.00003907	0.00004604	0.00001733
0.00000395	0.00001531	0.00003555	0.00004604	0.00007306	0.00004953
−0.00000186	0.00000087	0.00000708	0.00001733	0.00004953	0.00006542

References

Bailey, S. W., & Werdell, P. J. (2006). A multi-sensor approach for the on-orbit validation of ocean color satellite data products. *Remote Sensing of Environment*, *102*, 12−23.

Bezdek, J. C., Li, W. Q., Attikiouzel, Y., & Windham, M. (1997). A geometric approach to cluster validity for normal mixtures. *Soft Computing*, *1*, 166−179.

Hapke, B. (1981). Bidirectional reflectance spectroscopy 1. Theory. *Journal of Geophysical Research*, *86*, 3039−3054.

Hooker, S.B., Esaias, W.E., Feldman, G.C., Gregg, W.W., & McClain, C.R. (1992). An overview of SeaWiFS and ocean color, NASA Tech. Memo., vol. 104566. National Aeronautics and Space Administration, Goddard Space Flight Center.

Johnson, P. E., Smith, M. O., Taylor-George, S., & Adams, J. B. (1983). A semiempirical method for analysis of the reflectance spectra of binary mineral mixtures. *Journal of Geophysical Research*, *88*, 3557−3561.

McClain, C. R., Feldman, G. C., Hooker, S. B., & Bontempi, P. (2006). Satellite data for ocean biology, biogeochemistry, and climate research. *EOS Transactions*, *87*(34), 337−343.

Moore, T. S., Campbell, J. W., & Feng, H. (2001). A fuzzy logic classification scheme for selecting and blending satellite ocean color algorithms. *IEEE Transactions on Geoscience and Remote Sensing*, *39*, 1764−1776.

Morel, A., & Prieur, L. (1977). Analysis of variations in ocean color. *Limnology and Oceanography*, *22*(4), 709−722.

Mustard, J. M., & Pieters, C. M. (1989). Photometric phase functions of common geologic minerals and applications to quantitative analysis of mineral mixture reflectance spectra. *Journal of Geophysical Research*, *94*, 13,619−13,634.

O'Reilly, J.J. et al. (2000). SeaWiFS postlaunch calibration and validation analyses: Part 3, NASA Tech. Memo., vol. 206892. National Aeronautics and Space Administration, Goddard Space Flight Center.

Wang, F. (1990). Fuzzy supervised classification of remote sensing images. *IEEE Transactions on Geoscience and Remote Sensing*, *28*, 194−201.

Werdell, P. J., & Bailey, S. W. (2005). An improved in situ bio-optical data set for ocean color algorithm development and satellite data product validation. *Remote Sensing of Environment*, *98*, 122−140.

Wu, K. L., & Yang, M. S. (2005). A cluster validity index for fuzzy clustering. *Pattern Recognition Letters*, *26*, 1275−1291.